Uludağ University Journal of The Faculty of Engineering, Vol. 23, No. 3, 2018 RESEARCH

DOI: 10.17482/uumfd.333701

SIMULATION OF PHASE EQUILIBRIA IN HIGH CHROMIUM WHITE CAST IRONS

Öncü AKYILDIZ [*]
Duygu CANDEMİR [*]
Hakan YILDIRIM [**]

Received: 09.08.2017; revised: 10.08.2018; accepted: 08.11.2018

Abstract: In this study, using the Materials Calculator software program, the pseudo binary phase diagrams (i.e. isoplethal maps) of high chromium white cast irons (~19% in weight) with different molybdenum contents were simulated. In order to test the accuracy of the calculated phase diagrams, the transformation temperatures read from the diagrams at certain compositions were compared with the phase transformation temperatures measured using Differential Scanning Calorimetry (DSC) analysis of the samples produced by casting in the same composition followed by slow cooling. With the same purpose, low temperature phases read from the phase diagrams were compared with the crystalline phases determined by X-Ray Diffraction (XRD) of the casted samples. Simulated diagrams predicted an increase in the amount of secondary $M_{23}C_6$ carbides with increasing molybdenum content. The validity of this prediction was tested by determining the phase distribution and phase compositions in the casted samples by means of metallographic examinations and Scanning Electron Microscopy (SEM) - Energy Dispersive Spectroscopy (EDS) analyzes. When the hardness values of the samples were taken into consideration, it was seen that the hardness increased from 44.90 to 51.05 HRC with a 1% increase in Mo content and a corresponding increase in the amount of secondary carbides without any heat treatments. Results show that theoretical predictions and experimental measurements are in accord and estimating phase equilibria in multi-component systems is of practical importance.

Keywords: Computational thermodynamics, MatCalc, Alloy design, High chromium white cast iron, Secondary carbides

Yüksek Kromlu Beyaz Dökme Demirlerde Faz Dengesinin Benzetimi

Öz: Bu çalışmada Materials Calculator yazılımı kullanılarak, farklı molibden içeriğine sahip yüksek kromlu beyaz dökme demirlerin (ağırlıkça ~%19) ikilimsi faz diyagramları (eşdeğer kesit haritaları) benzetilmiştir. Hesaplanan faz diyagramlarının doğruluğunu test etmek amacı ile, diyagramlardan belirli kompozisyonlarda okunan dönüşüm sıcaklıkları, aynı kompozisyonlarda döküm sonrası yavaşça soğutularak üretilen numunelerin diferansiyel taramalı kalorimetri (İng.: Differential Scanning Calorimetry, DSC) analizi ile ölçülen faz dönüşüm sıcaklıkları ile karşılaştırılmıştır. Yine aynı amaçla, faz diyagramlarından okunan düşük sıcaklık fazları ve döküm ile üretilen numunelerin içindeki, X-ışını kırınım yöntemi (İng.: X-Ray Diffraction, XRD) ile belirlenen, kristalin fazlar karşılaştırılmıştır. Benzetilen diyagramlar, artan molibden içeriği ile ikincil $M_{23}C_6$ karbürlerin miktarında bir artış öngörmüştür. Bu öngörünün geçerliliği döküm ile üretilen numuneler içerisindeki faz dağılımı ve faz kompozisyonlarını metalografik muayene, taramalı elektron mikroskobu (İng.: Scanning Electron Microscopy, SEM) – enerji saçınım spektrometresi (İng.: Energy Dispersive Spectroscopy, EDS) analizleri ile belirleyerek test edilmiştir. Numunelerin sertlik değerlerine bakıldığında ise, herhangi bir ısıl

[*] Department of Metallurgical and Materials Engineering, Hitit University, 19030, Corum, Turkey.
[**] Duduoğlu Steel Casting Industry and Trade Inc. Co., 19040, Corum, Turkey.
Corresponding Author: Öncü AKYILDIZ (oncuakyildiz@hitit.edu.tr)

işlem yapılmaksızın Mo içeriğindeki %1 'lik bir artış ve buna bağlı ikincil karbürlerin miktarındaki artış ile sertliğin 44,90'dan 51,05 HRC'ye yükseldiği görülmüştür. Elde edilen sonuçlar deneysel ölçümler ve teorik tahminlerin uyumlu olduğunu ve çok bileşenli sistemlerde faz dengesinin tahmin edilebilmesinin pratik önemini göstermiştir.

Anahtar Kelimeler: Hesaplamalı termodinamik, MatCalc, Alaşım tasarımı, Yüksek kromlu beyaz dökme demir, ikincil karbürler

1. INTRODUCTION

White cast irons are hypoeutectic alloys in which the carbon remains dissolved in the carbide phases without decomposing into graphite during solidification. Because of the hard carbides, they preferred in high abrasion resistance required applications in mining, milling, earth-handling, and manufacturing industries (Su et al., 2006; Çetinkaya, 2003). In order to improve further the wear resistance, they usually alloyed with strong carbide forming elements (W, Mn, Mo, Cr, etc.). When the amount of alloying element exceeds 4%, they are referred as high-alloy white cast iron.

Chemical and hardness requirements for white cast irons suitable for applications requiring high abrasion resistance are specified in ASTM A532 standard (2014). High-alloy white cast irons conforming to this standard can be classified in three main classes. These are nickel – chromium, chromium – molybdenum and high chromium white cast irons. Nickel – chromium white cast irons contain 3.3 – 5 %Ni and 1 – 11 %Cr, chromium – molybdenum cast irons contain up to 3 %Mo and 12 – 23 %Cr, and high chromium white cast irons contain 23 – 30% Cr in mass percent. However, it is a common practice to name hypoeutectic alloys based on the ternary Fe-Cr-C system with compositions between 11 – 30 %Cr and 1.8 – 3.6% C as high chromium white cast irons (Jacuinde and Rainforth, 2001; Tabrett et al., 1996; Wiengmoon et al., 2005).

During solidification of high chromium white cast irons, primary austenite dendrites, followed by a eutectic mixture of austenite and M_7C_3 carbides or one of its transformation products form (Correa et al., 2011; Filipovic et al., 2011; Tabrett et al., 1996). The high amount of chromium in these alloys favor the formation of carbides (type M_7C_3 in between 9.5 to 15% Cr and $M_{23}C_6$ above 30 %Cr) and a pearlitic matrix in the absence of alloying additions (Abdel-Aziz et al., 2017; Wiengmoon et al., 2011; Zumelzu et al., 2003). Nickel, copper, and manganese are commonly added to improve hardenability and inhibit pearlite formation (Tabrett et al., 1996). Likewise, molybdenum is added to increase hardenability, but it also leads to the formation of other hard carbides apart from the M_7C_3 (Imuraiet al., 2015). The amount, type, size, shape and distribution of these carbides determine abrasion resistance of the material.

Phase diagrams are primary tools for determining the stable phases and their amounts on equilibrium cooling. Experimentally calculated phase diagrams are available only for simple binary and triple systems, whereas industrially produced alloys are composed of 10 or more components (Harding and Saunders, 1997). Today, various software programs (e.g. FactSage (Bale et al., 2009), MatCalc (Kozeschnik and Buchmayr, 2001), Pandat (Cao et al., 2009) and Thermo-Calc (Andersson et al., 2002)) are used to obtain thermodynamic calculations for multicomponent systems. Although, the features offered by the individual software packages differ, some modules, such as for the calculation of binary and ternary phase diagrams, are common to all software packages (Kattner, 2016). The MatCalc (The Materials Calculator) software program (Kozeschnik and Buchmayr, 2001) provides the ability to make thermodynamic as well as thermo-kinetic calculations for multicomponent systems. Its thermodynamic engine is based on the CALPHAD (CALculation of PHAse Diagrams) method and databases. The CALPHAD method provides the ability to simulate and generate phase diagrams to achieve a consistent approach to the determination of thermodynamic properties in the absence of experimental data in multi-component systems.

In this study, it was aimed to simulate the pseudo binary phase diagrams (i.e. isoplethal maps) of high chromium white cast irons (~19 %Cr in weight), containing different amounts of molybdenum, using MatCalc in order to assess the effect of molybdenum on the phase equilibria of these alloys. The calculated phase diagrams were validated by Differential Scanning Calorimetry (DSC) and X-Ray Diffraction (XRD) analysis of the casted samples produced by casting in the same composition followed by slow cooling. Simulated diagrams predicted an increase in the amount of $M_{23}C_6$ carbides with increasing molybdenum content. The validity of this prediction was also tested by determining the phase distribution and phase compositions in the casted samples by means of metallographic examinations and Scanning Electron Microscopy (SEM) - Energy Dispersive Spectroscopy (EDS) analyzes.

2. EXPERIMENTAL

The pseudo-binary phase diagrams of high chromium white cast iron alloys were simulated using MatCalc 6.00.0200 the Materials Calculator software program with database mc_fe_2.059.tdb. In order to validate the constructed phase diagrams, y-blocks (Figure 1) with two different compositions on the diagram, given in Table 1, were casted. Chemical analysis of the samples were performed by Thermo Scientific ARL 3460 optical emission spectrometer. Differential scanning calorimetry (DSC) analyses were carried out using the Toledo TGA/DSC 3+ for detecting the possible phase transformations. The samples with 10 – 40 mg were prepared and heated from room temperature to 1400 °C at a rate of 5 °C/min and then cooled to room temperature at the same rate. XRD analyses were performed using Rigaku Ultima IV X-ray diffractometer equipped with a Cu K-α source ($\lambda = 0.15406$ nm). Tests were carried out at 40 kV, 40 mA, and the Bragg angle (2θ) varied from 10 to 90° with a scan rate of 2°/min.

For microstructural analysis, white cast iron samples were encapsulated in a round bakelite (Metkon-Phenolic resin powder) mount with a diameter of 4 cm. The specimens were mechanically grinded with 180 to 1200 grit SiC paper then polished with 1µm diamond suspension to mirror finish (Metkon Forcipol 1V Grinder-Polisher). Finally, the samples were etched with Nital reagent (2–4 mL nitric acid (HNO3) and 96–98 mL ethanol). After the metallographic treatments, specimens were cleaned in an ultrasonic bath using ethanol for 10 min and then dried. The microstructures of the specimens were investigated by using an optical microscope (Nikon ECLIPSE LV150N). Hardness measurements were performed with Krautkramer DynaMIC instrument. SEM - EDS analyzes were performed by FEI / Quanta 450 FEG scanning electron microscope and energy scattering spectrometer.

Table 1. Elemental compositions of the tested alloys determined using optical emission spectrometry.

Sample name	Chemical composition (mass %)											Sum (%)
	C	Si	Mn	P	S	Cr	Mo	Ni	V	Al	Cu	
9640	2.95	0.69	0.65	0.02	0.02	19.14	0.48	0.24	0.06	0.13	0.09	24.51
9645	2.86	0.67	0.70	0.02	0.02	19.72	1.57	0.23	0.06	0.03	0.10	26.04

Figure 1:
Rectangular blocks (20x4x4 cm; ca. 5 kg) cut from y-blocks (ca. 35 kg) of different compositions.

2. RESULTS and DISCUSSION

The calculated pseudo binary phase diagrams for the two alloy systems given in Table 1 is presented in Figure 2. From these diagrams, it is found that the eutectic point temperature and carbon content are 1281 °C and 3.21% for alloy 9640, respectively, whereas the corresponding values for alloy 9645 are 1275 °C and 3.20%. Note that the eutectic transition temperature is increased and the content of eutectic carbon is decreased compared to the unalloyed white cast iron (1147 °C and 4.3 %C). This alloying affect favors the presence of higher proportion of stable chromium carbides (Higuera-Cobos et al., 2015). The primary austenite phase nucleates and grows as the alloy 9640 (with 2.95 %C) cools down to 1282 °C as shown in Figure 2a-3a. The transformation start temperature read from the phase diagram is 1298 °C (Figure 2a), which is very close to the exothermic peak temperature at 1310 °C (Figure 3b, peak # 1). Afterwards, a eutectic reaction L → γ + M_7C_3 occurs at 1282 °C and finishes at 1238 °C which are also close to the DSC peaks # 2 and 3. In between 1238 and 802 °C austenite and M_7C_3 phases coexist. At 802 °C the eutectoid reaction γ → α + M_7C_3 occurs and leaves a two phase α + M_7C_3 structure after 778 °C. These eutectoid-transformation-start and finish temperatures are also very close to the DSC peaks # 4 and 5 given in Figure 3b. For lower temperatures there still exists a certain level of agreement as observed by Li et al. (2009) and Yen et al. (2013).

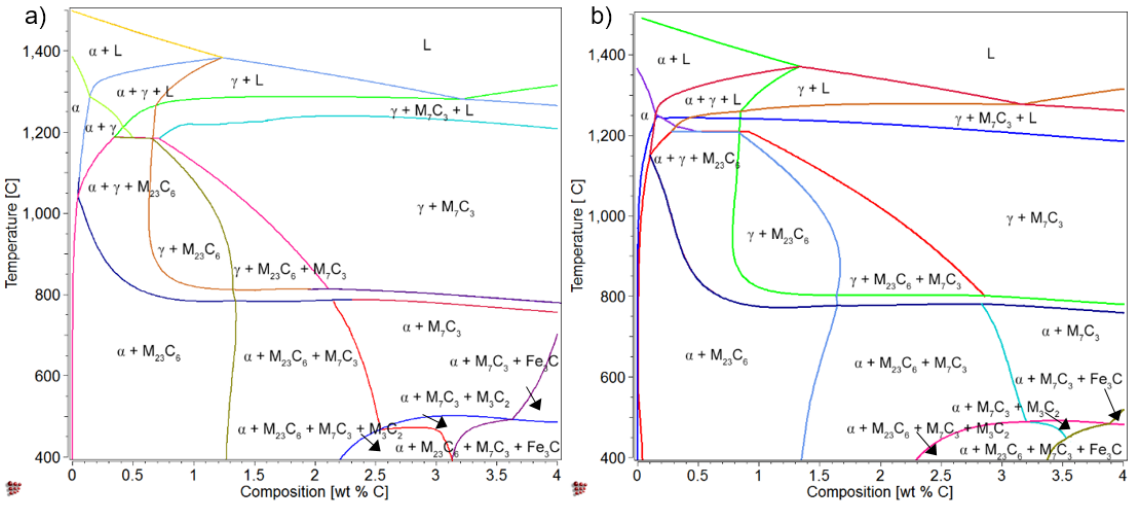

Figure 2:
Pseudo-binary phase diagram for samples;
a. *9640* ***b.*** *9645*

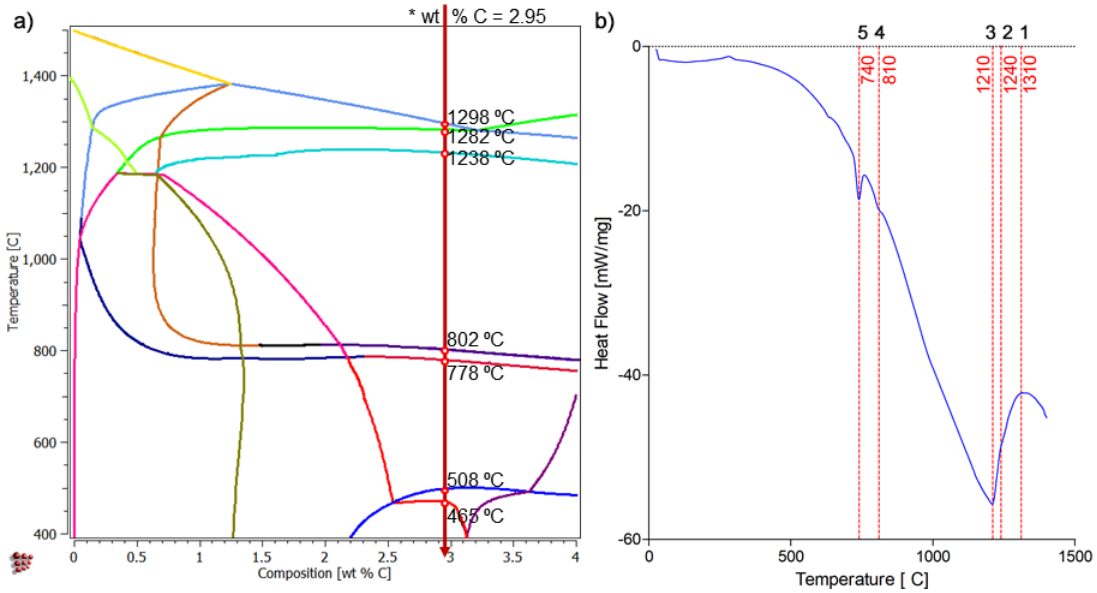

Figure 3:

a. *phase boundaries at 2.95 weight % carbon for alloy 9640* ***b.*** *differential scanning calorimetry curve for the same alloy.*

The presence of low temperature phases, read from the phase diagrams, were checked in the samples produced by the casting by the X-ray diffraction analysis given in Figure 4.

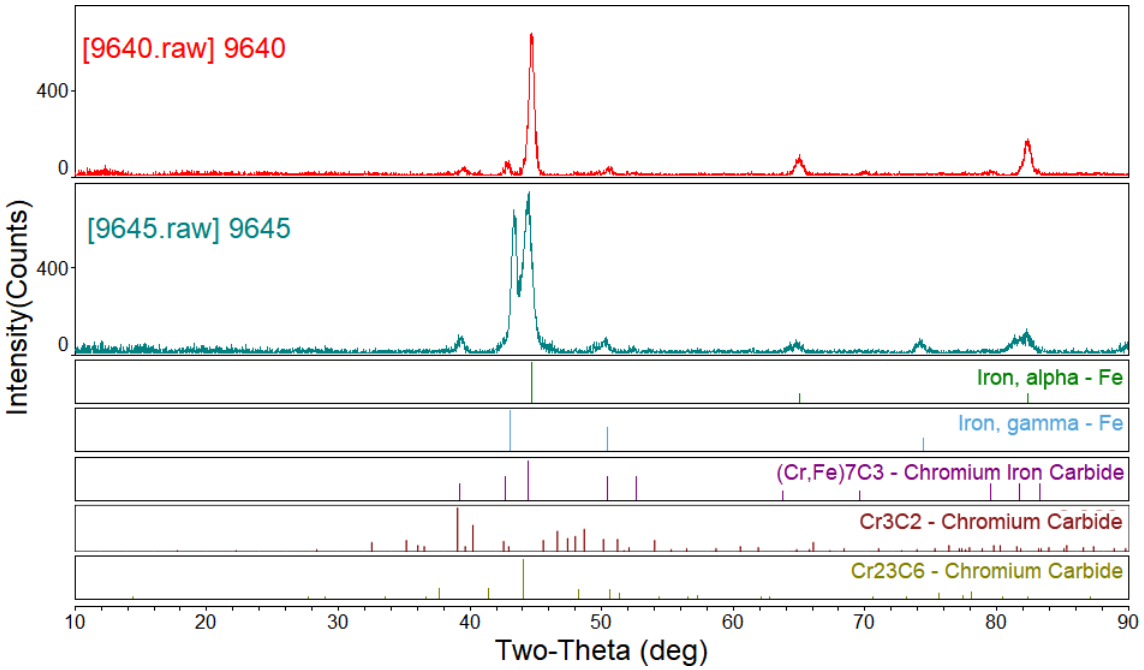

Figure 4:

X-ray diffraction patterns for samples 9640 and 9645.

Looking at Figure 4, it appears that ferrite (α-Fe) and austenite (γ-Fe) peaks are evident in both samples. The as cast microstructure of high chromium white cast irons usually reported to have a metastable austenitic matrix (Bedolla-Jacuinde et al., 2005; Filipovic et al., 2011; Li et al., 2009; Tabrett et al., 1996). Yet, the presence of ferrite (in lower amounts than austenite) was also reported in literature (Higuera-Cobos et al., 2015) as is observed herewith. From MatCalc one can also track the chemical compositions of the carbides, which are presented in Table 2. From the chemical compositions presented in Table 2, it can be seen that the equilibrium composition of the M_7C_3 phase should be a Cr-rich (Cr, Fe, Mn, Mo)$_7C_3$ type carbide phase. Accordingly, Figure 4 confirms presence of (Fe, Cr)$_7C_3$ type carbides. The M_3C_2 phase according to Table 2 must be Cr_3C_2 for both alloys. The peak at $2\theta = 39.4^o$, which is the strongest peak in the diffraction pattern of these carbides shown in Figure 4, is apparent in both samples. Similarly, due to Table 2, the $M_{23}C_6$ phase should be a (Fe, Cr, Mo, Mn)$_{23}C_6$ type carbide phase. In Figure 4, the peak at $2\theta = 44.4^o$, which is the strongest peak in the diffraction pattern for $Cr_{23}C_6$ phase, coincides with the α - Fe peak, and the peak at $2\theta = 74.3^o$ in alloy 9645 is located close to the peak belonging to this carbide.

Table 2. Phase details: Chemical composition of the carbides in low Mo (9640) and high Mo (9645) alloys.

Carbide	Alloy #	Chemical composition (mol %)					
		C	Fe	Cr	Mo	Mn	V
M_3C_2	9640	40	-	59.81	-	-	0.19
	9645	40	-	59.85	-	-	0.15
M_7C_3	9640	30	15.18	43.28	1.35	9.94	0.22
	9645	30	14.83	53.51	0.13	1.19	0.34
$M_{23}C_6$	9640	20.69	35.48	33.20	9.84	0.62	-
	9645	20.69	38.30	32.61	8.19	0.19	-

Comparing Figures 2a and b suggests that increasing the Mo amount shifts the $M_{23}C_6/M_7C_3$ boundaries towards higher carbon concentrations on an isotherm and in this respect, Mo act as a $M_{23}C_6$ stabilizer. For example, an isotherm drawn at 900 °C crosses the $\gamma+M_{23}C_6/\gamma+M_{23}C_6+M_7C_3$ phase boundary at 1.25 %C for alloy 9640, whereas it is 1.6 %C for alloy 9645. Similarly, for $\gamma+M_{23}C_6+M_7C_3/\gamma+M_7C_3$ phase boundary the values are 1.75 and 2.35 %C respectively for 9640 and 9645. Medvedeva et al. were also predicted tungsten and molybdenum additions stabilize the binary $M_{23}C_6$ (M = Cr, Fe, Co, Ni) and ternary (Cr,M)$_{23}C_6$ (M = Fe, Ni) carbides by using first principles calculations (Medvedeva et al., 2015). This effect is best illustrated in Figure 5. The calculated volumetric equilibrium phase fractions show that $M_{23}C_6$ starts to form at 770 °C in high Mo (9645) alloy compared to 470 °C in low Mo (9640) alloy. The final phase fraction of $M_{23}C_6$ in 9645 is about 10 %, which is almost five times higher than 9640.

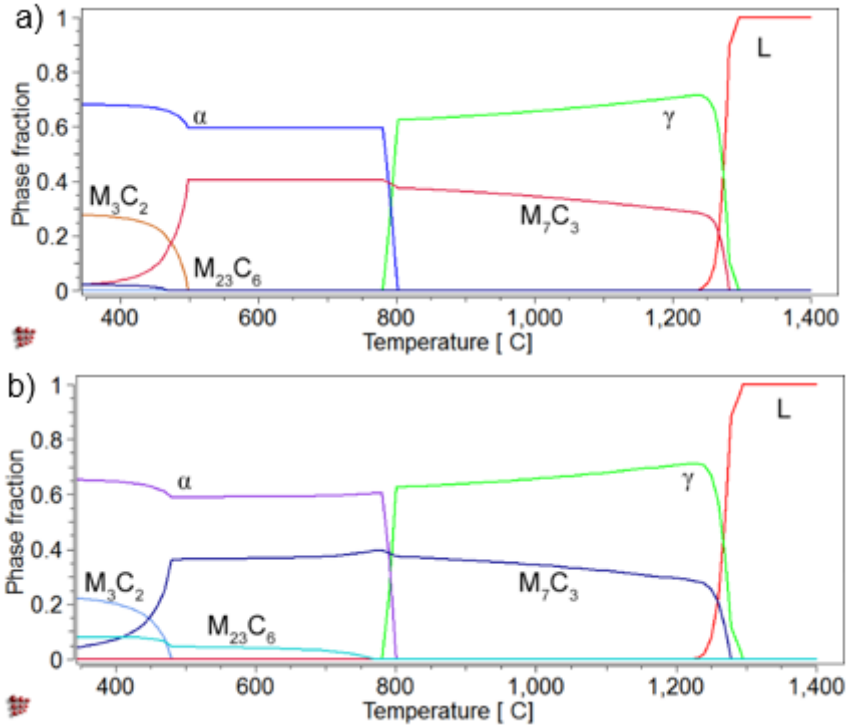

Figure 5:
Calculated equilibrium phase fractions for samples;
a. *9640* ***b.*** *9645*

The microstructure of the alloys were investigated with optical microscopy. Figure 6 shows that the 9640 alloy has a coarser structure with discontinuous carbides whereas the 9645 alloy has finer structure. The refining mechanism may be attributed to the lower eutectic transformation temperature due to higher amount of molybdenum in alloy 9645. The lower the carbide formation temperature, the higher the nucleation undercooling (i.e. increased driving force for nucleation or increased number of nuclei's) and the finer the structure. Conversely, the growth rate of the eutectic carbide colonies decreases with decreasing eutectic temperature. The increase of the nucleation rate and the decrease of the growth rate of the eutectic colonies together lead to small carbide spacing (Mampuru et al., 2016; Ogi et al., 1982; Youping et al., 2012). Furthermore, in higher magnification (Figure 6f) finely distributed secondary carbides were identified within the austenitic matrix of alloy 9645. In order to gain information on these secondary carbides, alloy 9645 was subjected to SEM - EDS analysis. Results of the EDS point analyses on four different points shown in Figure 7 is presented in Table 3. When these measurements are examined, it is seen that the primary carbides marked in Figure 7ab are Cr-rich and the secondary carbides marked in Figure 7cd are in Fe-rich structure. These observations are consistent with the chemical compositions of the carbides previously presented in Table 2 (Cr-rich M_7C_3, Fe-rich $M_{23}C_6$).

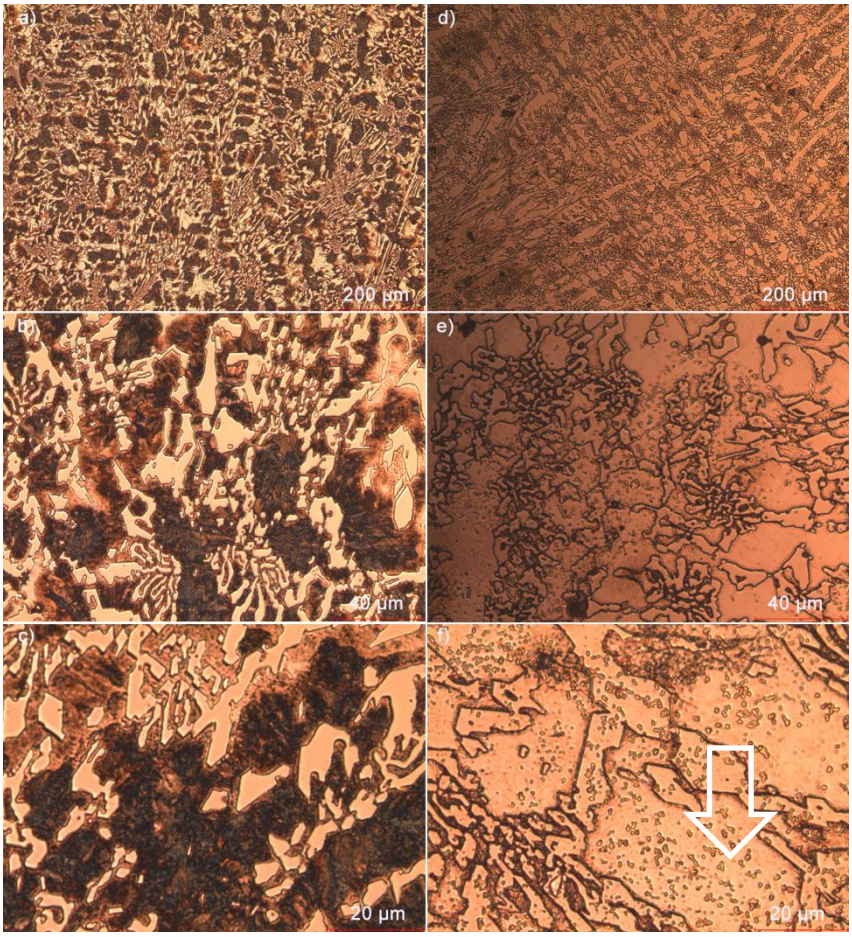

Figure 6:
Metallographic examination results for sample 9640 at ***a.*** *10x,* ***b.*** *50x, and* ***c.*** *100x, and for sample 9645 at* ***d.*** *10x,* ***e.*** *50x, and* ***f.*** *100x magnification where finely distributed $M_{23}C_6$ secondary carbides are marked within the austenitic matrix and eutectic M_7C_3 carbide colonies.*

Table 3: Chemical compositions from EDS analysis of alloy 9645

Point	Chemical composition (weight %)			
	Fe	Cr	Mn	Mo
a	43.72	52.35	1.68	2.25
b	42.91	53.55	1.51	2.03
c	76.62	20.27	1.38	1.74
d	75.68	20.42	2.07	1.86

The basic physical property correlating with wear resistance of white cast irons is hardness (Heino et al., 2017). According to Archard's law (Archard, 1953), the material lost by abrasive wear is inversely proportional to the hardness, in other words the hardness and abrasion resistance are directly proportional. For this reason, measurements were taken to see the effect of the increase in the amount of secondary carbides on material hardness. The measured hardness values in Rockwell scale are given in Table 4. From this data it is seen that hardness is

increased from 44.90 to 51.05 HRC with a ~ 1% increase in Mo content due to the microstructural modification presented in Figure 6 without any heat treatments.

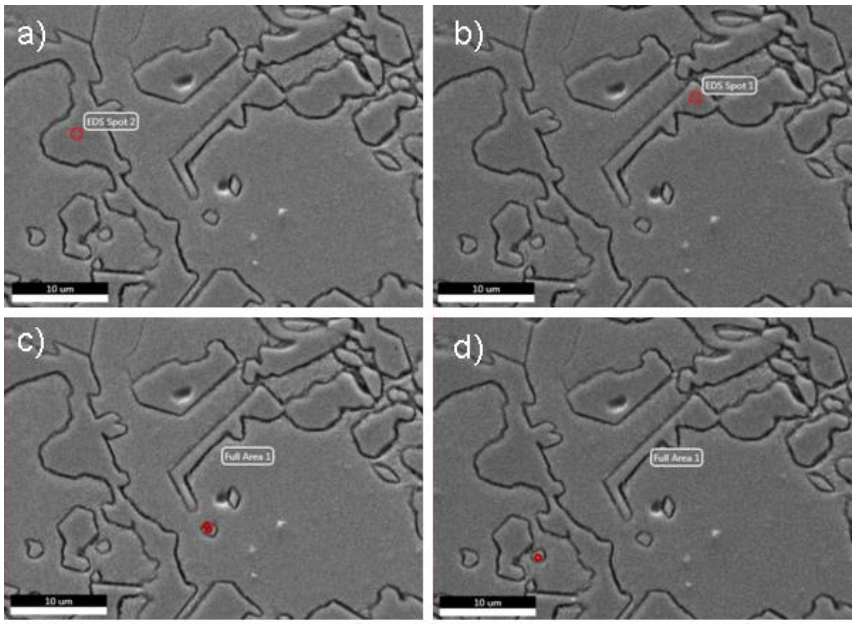

Figure 7:
SEM image of the sample 9645 and four points where the point EDS analysis is made: a) and b) primary carbides, c) and d) secondary carbides.

Table 4. Measured hardness values in Rockwell scale.

Sample name	C	Cr	Mo	HRC
9640	2.95	19.14	0.48	44.90
9645	2.86	19.72	1.57	51.05

3. CONCLUSION

In this work, which is an example of the use of CALPHAD based computational techniques in the design of high chromium white cast iron alloys, binary phase diagrams have been simulated for multicomponent alloy systems with different molybdenum content and the resulting diagrams have been verified experimentally (by DSC and XRD analysis). Simulated pseudo binary phase diagrams predicted an increase in the amount of $M_{23}C_6$ carbides with increasing molybdenum content. Metallographic examinations confirm the existence of finely distributed secondary $M_{23}C_6$ carbides within the austenitic matrix phase of high molybdenum content sample, which results in an increase in the hardness of the sample. SEM - EDS analyzes show that these carbide phases are Fe - rich in conformity with theoretical predictions. The MatCalc application environment not only provides thermodynamics calculations but also paves way to multicomponent, multiphase kinetics calculations. Solid state precipitation kinetics during heat treatments are left as a future work.

Acknowledgements

Thanks are due to Mr. Mustafa Duduoğlu, Chairman of the Board of Directors of Duduoğlu Steel Casting Industry Trade Inc. for his constant support and interest in this work. This work

was supported by the Hitit University Scientific Research Projects Funding Program through a research Grant No. MUH19001.16.006.

REFERENCES

1. Abdel-Aziz, K., El-Shennawy, M., Omar, A. A. (2017) Microstructural Characteristics and Mechanical Properties of Heat Treated High-Cr White Cast Iron Alloys, *International Journal of Apllied Engineering Research*, 12, 4675–4686.

2. Andersson, J. O., Helander, T., Höglund, L., Shi, P., & Sundman, B. (2002) Thermo-Calc & DICTRA, computational tools for materials science. *Calphad: Computer Coupling of Phase Diagrams and Thermochemistry*, 26(2), 273–312. doi:10.1016/S0364-5916(02)00037-8

3. Archard, J. F. (1953) Contact of rubbing flat surfaces, *Journal of Applied Physics*, 24, 981–988. doi: 10.1063/1.1721448

4. ASTM A532 / A532M-10(2014), (2014). Standard Specification for Abrasion-Resistant Cast Irons, ASTM International, West Conshohocken, PA. doi: 10.1520/A0532_A0532M-10R14

5. Bale, C. W., Bélisle, E., Chartrand, P., Decterov, S. A., Eriksson, G., Hack, K., Petersen, S. (2009). FactSage thermochemical software and databases - recent developments, *Calphad: Computer Coupling of Phase Diagrams and Thermochemistry*, 33(2), 295–311. doi: 10.1016/j.calphad.2008.09.009

6. Bedolla-Jacuinde, A., Hernández, B., and Béjar-Gómez, L. (2005) SEM study on the M7 C3 carbide nucleation during eutectic solidification of high-chromium white irons, *Zeitschrift Für Metallkunde*, 96(12), 1380–1385. doi: 10.3139/146.101188

7. Cao, W., Chen, S. L., Zhang, F., Wu, K., Yang, Y., Chang, Y. A., … Oates, W. A. (2009) PANDAT software with PanEngine, PanOptimizer and PanPrecipitation for multi-component phase diagram calculation and materials property simulation, *Calphad: Computer Coupling of Phase Diagrams and Thermochemistry*, 33(2), 328–342. doi: 10.1016/j.calphad.2008.08.004

8. Çetinkaya, C. (2003) Yüksek kromlu beyaz dökme demir malzemelerin Al2O3 ile aşınma davranışlarının incelenmesi, *Politeknik Dergisi*, 6(3) 559-567.

9. Correa, R., Bedolla-Jacuinde, A., Mejía, I., Cardoso, E., and Hernández, B. (2011) Effect of boron on microstructure of directionally solidified high chromium white irons, *International Journal of Cast Metals Research*, 24(1), 37–44. doi: 10.1179/136404611X12965641181767

10. Filipovic, M., Kamberovic, Z., & Korac, M. (2011) Solidification of High Chromium White Cast Iron Alloyed with Vanadium, *Materials Transactions*, 52(3), 386–390. doi: 10.2320/matertrans.M2010059

11. Harding, R.A., Saunders, N.J. (1997) Theory and Practice of Computer Modelling of Phase Diagrams for Cast Irons, *Trans. American Foundrymen's Society*, 105, 451-457.

12. Heino, V., Kallio, M., Valtonen, K., Kuokkala, V.-T. (2017) The role of microstructure in high stress abrasion of white cast irons, *Wear*, 388–389, 119–125. doi: 10.1016/j.wear.2017.04.029

13. Higuera-Cobos, O. F. (2015) Improvement of abrasive wear resistance of the high chromium cast iron ASTM A-532 through thermal treatment cycles, *Facultad de Ingeniería*, 25(41), 93–103.

14. Imurai, S., Thanachayanont, C., Pearce, J. T. H., & Chairuangsri, T. (2015) Microstructure

And Erosion-Corrosion Behaviour Of As-Cast High Chromium White Irons Containing Molybdenum In Aqueous Sulfuric-Acid Slurry, *Archives of Metallurgy and Materials*, 60(2), 919–923. doi: 10.1515/amm-2015-0230

15. Jacuinde, A. B., & Rainforth, W. M. (2001) The wear behaviour of high-chromium white cast irons as a function of silicon and Mischmetal content, *Wear*, 250–251(PART 1), 449–461. doi: 10.1016/S0043-1648(01)00633-0

16. Kattner, U. R. (2016) the Calphad Method and Its Role in Material and Process Development. *Tecnologia Em Metalurgia Materiais e Mineração*, 13(1), 3–15. doi: 10.4322/2176-1523.1059

17. Kozeschnik E, Buchmayr B. (2001) MatCalc - a simulation tool for multicomponent thermodynamics, diffusion and phase transformation kinetics, *Mathematical modelling of weld phenomena 5*, London Institute of Materials, UK, 349-361.

18. Li, D., Liu, L., Zhang, Y., Ye, C., Ren, X., Yang, Y., Yang, Q. (2009) Phase diagram calculation of high chromium cast irons and influence of its chemical composition, *Materials and Design*, 30(2), 340–345. doi: 10.1016/j.matdes.2008.04.061

19. Mampuru, L. A., Maruma, M. G., & Moema, J. S. (2016) Grain refinement of 25 wt% high-chromium white cast iron by addition of vanadium, *Journal of the Southern African Institute of Mining and Metallurgy*, 116(10), 969–972. doi: 10.17159/2411-9717/2016/v116n10a12

20. Medvedeva, N. I., Van Aken, D. C., & Medvedeva, J. E. (2015) Stability of binary and ternary M23C6carbides from first principles, *Computational Materials Science*, 96(PA), 159–164. doi: 10.1016/j.commatsci.2014.09.016

21. Ogi K, Matsubara Y, and Matsuda K. (1982) Eutectic solidification of high chromium cast iron-eutectic mechanism of eutectic growth, *AFS Transactions*, 89, 197–204.

22. Su, Y-L., Li, D., Zhang, X-E. (2006) Optimizing hardenability of high chromium white cast iron, *China Foundry*, 3(4), 284-287.

23. Tabrett, C. P., Sare, I. R., & Ghomashchi, M. R. (1996) Microstructure-property relationships in high chromium white iron alloys, *International Materials Reviews*, 41(2), 59–82. doi: 10.1179/095066096790326075

24. Wiengmoon, A., Chairuangsri, T., & Pearce, J. T. H. (2005) An unusual structure of an as-cast 30% Cr alloy white iron, *ISIJ International*, 45(11), 1658–1665. doi: 10.2355/isijinternational.45.1658

25. Wiengmoon, A., Pearce, J. T. H., & Chairuangsri, T. (2011) Relationship between microstructure, hardness and corrosion resistance in 20 wt.%Cr, 27 wt.%Cr and 36 wt.%Cr high chromium cast irons, *Materials Chemistry and Physics*, 125(3), 739–748. doi: 10.1016/j.matchemphys.2010.09.064

26. Yen, C. L., Liu, K. L., & Pan, Y. N. (2013) Simulation of the Phase Diagrams for High-Chromium White Cast Irons and Multi-Component White Cast Irons, *Advanced Materials Research*, 848, 39–45. doi: 10.4028/www.scientific.net/AMR.848.39

27. Youping, M., Xiulan, L., Yugao, L., Shuyi, Z., & Xiaoming, D. (2012) Effect of Ti-V-Nb-Mo addition on microstructure of high chromium cast iron, *China Foundry*, 9(2), 148–153.

28. Zumelzu, E., Opitz, O., Cabezas, C., Parada, A., & Goyos, L. (2003) High-chromium (22-34 percent) cast iron alloys and their simulated behaviour at the sugar industry, *Journal of Scientific and Industrial Research*, 62(6), 583–588.